Computational modelling of optical tweezers with many degrees of freedom using dynamic simulation: cylinders, nanowires, and multiple particles

Yongyin Cao[a,b,*], Alexander B Stilgoe[b], Martin Stroet[b], Vincent L. Y. Loke[b], Lixue Chen[a], Timo A. Nieminen[b], and Halina Rubinsztein-Dunlop[b]

[a]Department of Physics, School of Science, Harbin Institute of Technology, Harbin, 150001, China
[b]School of Mathematics and Physics, The University of Queensland, Brisbane, QLD 4072, Australia

ABSRACT

Computational tasks such as the calculation and characterization of the optical force acting on a sphere are relatively straightforward in a Gaussian beam trap. Resulting properties of the trap such as the trap strength, spring constants, and equilibrium position can be easily determined. More complex systems with non-spherical particles or multiple particles add many more degrees of freedom to the problem. Extension of the simple methods used for single spherical particles could result in required computational time of months or years. Thus, alternative methods must be used. One powerful tool is to use dynamic simulation: model the dynamics and motion of a particle or particles within the trap. We demonstrate the use of dynamic simulation for non-spherical particles and multi-particle systems. Using a hybrid discrete dipole approximation (DDA) and T-matrix method, we find plausible equilibrium positions and orientations of cylinders of varying size and aspect ratio. Orientation landscapes revealing different regimes of behaviour for micro-cylinders and nanowires with different refractive indices trapped with beams of differing polarization are also presented. This investigation provides a solid background in both the function and properties of micro-cylinders and nanowires trapped in optical tweezers. This method can also be applied to particles with other shapes. We also investigate multiple-particle trapping, which is quite different from single particle systems, as they can include effects such as optical binding. We show that equilibrium positions, and the strength of interactions between particles can be found in systems of two and more particles.

Key words: Optical trapping, optical tweezers, nanowire, DDA, multiple scattering, point matching

1. INTRUDCTION

Since Ashkin's work for optical tweezers in the 1970s [1], optical trapping has been widely used in physics, biology and chemistry [2-4]. Spherical particles have few degrees of freedom, therefore it's much easier to understand the trapping and the effect of manipulating such particles is easily to inflict. The calculation for optical trapping of spheres, such as the axial and radial trap strengths and spring constants, can be easily done by Lorenz-Mie theory [5,6]. The microspheres have found widespread in use as handles or probes and continued to be popular objects of optical trapping. However, many other non-spherical particles, such as crystals, single cells or some fabricated non-spherical particles, have been trapped or manipulated in optical tweezers. Computational modelling for the optical trapping of such particles is significantly more difficult than for spherical particles. Compared with the analytical solution for spheres, the analytical solution for non-spherical particles cannot be obtained. Numerical methods need to use to solve the scattering problem. There are many methods that can be used to model such optical trapping. One of the most efficient methods is T-matrix method. There are two degrees of freedom in orientation (for axisymmetric particles) or three degrees of freedom otherwise required to describe the orientation of the particle. In addition, the single spheres are always trapped on the beam axis in a Gaussian beam. Non-spherical particles will not necessarily be centred on the beam axis.

One more interesting class of non-spherical particles is elongated nanoparticles, which often have subwavelength cross-sections. Optical trapping and manipulation of such particles have been observed and exploited in aqueous environments [7,8]. It is of great interest to investigate the trapping of nanostructures and to discuss their orientations and rotations. As

* yongyincao@gmail.com

Optical Trapping and Optical Micromanipulation IX, edited by Kishan Dholakia, Gabriel C. Spalding, Proc. of SPIE Vol. 8458, 84582V · © 2012 SPIE · CCC code: 0277-786/12/$18 · doi: 10.1117/12.930137

it affects interaction with the environment, the optical force and torque, and the translational and rotational viscous tensors are required to be calculated for this purpose. However, the methods, such as such as DDA, finite difference frequency domain (FDFD) or extended boundary condition method (EBCM), don't work for single elongated particles with a large aspect ratio or will take a significantly long time to simulate the movements. If the nanowire with a large aspect ratio is calculated using DDA, for instance, it requires a large number of dipoles and the size of dipoles smaller than 1/10 of the radius [9]. In addition, multiple particles can be trapped in holographic tweezers or sometimes in a single tightly focused laser beam, where the effects of optical binding should be considered [10]. Some calculations for multiple-particle systems exist under the condition that the particles are not extremely close to one another. A new method is required to solve this problem when the particles are very close.

In this paper, we develop a model for single particles to simulate the trapping process and apply it to micro- and nano-cylinders. The force and torque on dielectric cylinders in a tightly focused Gaussian beam are calculated using T-matrix method based on discrete dipole approximation [11-14] for single cylinders. Another interesting goal is to develop a model for multiple-particle systems, which is quite different from the model for single particle systems. A two-sphere system is dynamically simulated using tangential field point-matching method [15,16]. The axial forces of a multiple-cylinder system are calculated as well.

2. THEORY

2.1 Theory for single particle systems

Optical fields can be expanded in terms of incident and scattered field potentials, which can be written as the sums of wave functions in different modes (Ψ_n^{inc} and Ψ_k^{scat}). There is a relationship between the incident and scattered fields

$$\tilde{\mathbf{P}}=\mathbf{T}\tilde{\mathbf{A}}, \tag{1}$$

where $\tilde{\mathbf{P}}$ and $\tilde{\mathbf{A}}$ are vectors of the beam shape coefficients of incident and scattered fields. $\mathbf{T}$ is the transition matrix of a particle. We label two components of the beam expansion coefficients of the incident field as $\mathbf{a}_0$ and $\mathbf{b}_0$, which are the TE/TM modes of $\tilde{\mathbf{A}}$ in the Cartesian coordinate system centred on the beam focus. The coefficients in an arbitrary coordinate system centred at any position can be found using a linear transformation [11,17,18],

$$\mathbf{a}=\mathbf{R}_2\left(\mathbf{R}_1^{-1}\mathbf{A}\mathbf{R}_1\mathbf{a}_0+\mathbf{R}_1^{-1}\mathbf{B}\mathbf{R}_1\mathbf{b}_0\right), \tag{2}$$

$$\mathbf{b}=\mathbf{R}_2\left(\mathbf{R}_1^{-1}\mathbf{B}\mathbf{R}_1\mathbf{a}_0+\mathbf{R}_1^{-1}\mathbf{A}\mathbf{R}_1\mathbf{b}_0\right). \tag{3}$$

Where $\mathbf{a}$ and $\mathbf{b}$ are the coefficients of the incident field in the new orthogonal coordinate system. $\mathbf{R_1}$ and $\mathbf{R_2}$ are the rotation of beam shape coefficients as shown in Fig. 1. $\mathbf{A}$ and $\mathbf{B}$ are the translations of beam coefficients in the rotated coordinate system along $\mathbf{O_1O_2}$. When the beam shape coefficients in particle-orientated frame are obtained, the coefficients of the scattered field, $\mathbf{p}$ and $\mathbf{q}$ (the TE/TM modes of $\tilde{\mathbf{P}}$), can be found by Eq. (1).

A particle near the focal region will "fall" into the trap at the equilibrium position with a stable orientation as a result of optical force and torque. The force and torque acting on the particle, $\mathbf{F}$ and $\mathbf{\Gamma}$, are calculated using optical tweezers computational toolbox [19]. All the micro- or nano-particles in our calculations are at low Reynolds number [20], therefore we consider the viscous drag exerted on the particle as opposing the optical force, and that the viscous torque opposes the radiation torque. Given the force, torque, position and orientation at time t, the particle's next position and orientation after a short time interval can be obtained using the following equations

$$\boldsymbol{v}=\boldsymbol{\gamma}_{\text{t}}^{-1}\mathbf{F}, \tag{4}$$

$$\boldsymbol{\omega}=\boldsymbol{\gamma}_{\text{r}}^{-1}\mathbf{\Gamma}, \tag{5}$$

$$\boldsymbol{r}\left(t+\text{d}t\right)=\boldsymbol{r}\left(t\right)+\boldsymbol{v}\,\text{d}t, \tag{6}$$

$$\mathbf{R}_{2,3,t+\text{d}t}=\Delta\mathbf{R}\mathbf{R}_{2,3,t}. \tag{7}$$

Where $\boldsymbol{v}$ and $\boldsymbol{\omega}$ are velocity and angular velocity of the particle at time t, $\boldsymbol{r}$ is the position of the centre of mass, $\boldsymbol{\gamma}_t$ and $\boldsymbol{\gamma}_r$ are the translational and rotational viscous friction tensors for the particle respectively. dt is generally a time interval between 10^{-4}~10^{-3} s. $R_{2,3,t}$ and $R_{2,3,t+dt}$ are the rotation matrices of the particle at time t and t+dt, which represent the orientations of the particle. $\Delta\mathbf{R}$ is found using the Euler-Rodrigues formula for axis angle rotations [21].

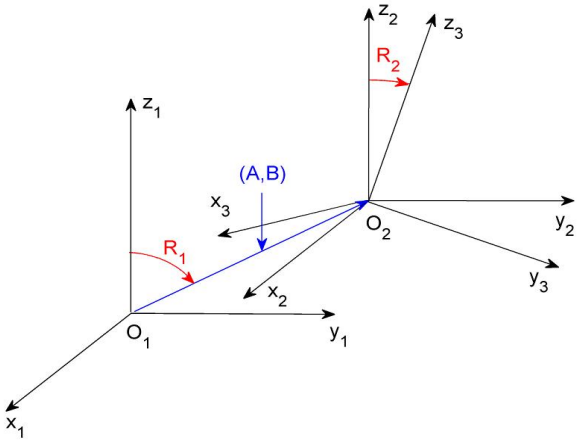

Figure 1. Rotations and translations of beam coefficients from the Cartesian coordinate system $x_1y_1z_1$ centred on the beam focus to an arbitrary coordinate system $x_3y_3z_3$ in particle frame. $\mathbf{R_1}$ and $\mathbf{R_2}$ are the rotations of beam coefficients. **A** and **B** are the translations of beam coefficients along $\mathbf{O_1O_2}$ direction.

2.2 Multiple scattering

For the multiple-particle systems, the effects of multiple scattering should be considered. When the group of particles are not close to one another, multiple scattering is weak. The solution of the electromagnetic field is well approximated by the sum of the external field and the field scattered by each particle in the absence of other particles. The scattering field of each particle can be found by Eq. (1). Therefore, the incident field for each scatterer can be written as [11,22]

$$\mathbf{a}_k^i = \mathbf{a}_{k0}^i + \sum_{j\neq k} \mathbf{a}_{js}^i, \tag{8}$$

$$\mathbf{b}_k^i = \mathbf{b}_{k0}^i + \sum_{j\neq k} \mathbf{b}_{js}^i. \tag{9}$$

Where i is the time step, j and k represent the j^{th} and k^{th} scatterers. $\mathbf{a}_{k0}$ and $\mathbf{b}_{k0}$ are the beam coefficients of the incident field for the k^{th} scatterer without considering other scatterers. $\mathbf{a}_{js}$ and $\mathbf{b}_{js}$ are the beam coefficients of the scattering field for the j^{th} scatterer. The iterative process continues until the scattering field of each scatterer converges. The forces and torques can then be obtained. The theory of multiple scattering works well when the particles are not very close to one another. However, there are few reports for solving the problem when the particles are extremely close or stuck to one another. We combine the theory of multiple scattering and point matching to solve this problem.

3. RESULTS

A single tightly focused Gaussian beam was used in our calculations, which was focused by high numerical aperture lens (NA = 1.25). The beam propagated along the $+z_1$ direction with its focus located at the origin $\mathbf{O_1}$ as shown in Fig. 1. The wavelength chosen for the beam was λ = 800 nm in water. The power going through the focal plane was P_{inc} = 1 mW.

3.1 Orientation landscapes for single cylinders

The equilibrium positions and orientations of cylinders of varying size and aspect ratio can be easily obtained using the model outlined in section 2. Since the translational and rotational friction tensors for cylinders given by Delatorre and Bloomfield [23] only apply to aspect ratio of length to diameter greater than one, we did not perform calculations for disks (aspect ratio < 1). We reformed calculations for micro- and nano-cylinders with diameters less than 500 nm and lengths less than 3000 nm. Orientation landscapes for micro-cylinders and nanowires with different refractive indices trapped in linearly and circularly polarized beams are presented in Fig. 2. The polarizations of the beams in Fig. 2a, 2c and 2e are linear polarization. The beams for Fig. 2b, 2d and 2f are circularly polarized. There are four regimes in the orientation landscapes for cylinders: a horizontal region, vertical region, an intermediate region between the vertical and

horizontal regions, and an untrapped region. In general, particles with large sizes or high-indices possibly can't be trapped. The cylinders in the horizontal and vertical regions are oriented to the horizontal and vertical directions respectively. The cylinders in the intermediate region can be trapped with a tilt angle between 0 and 90 degrees from the beam axis. There is no untrapped region for the cylinders with refractive index of 1.38 as shown in Fig. 2a and 2b. There is a small untrapped region for cylinders in Fig. 2c and 2d, of which the refractive index is 1.57. The untrapped region for the silicon cylinders with a very high refractive index (3.5498) is much larger as shown in Fig. 2e and 2f.

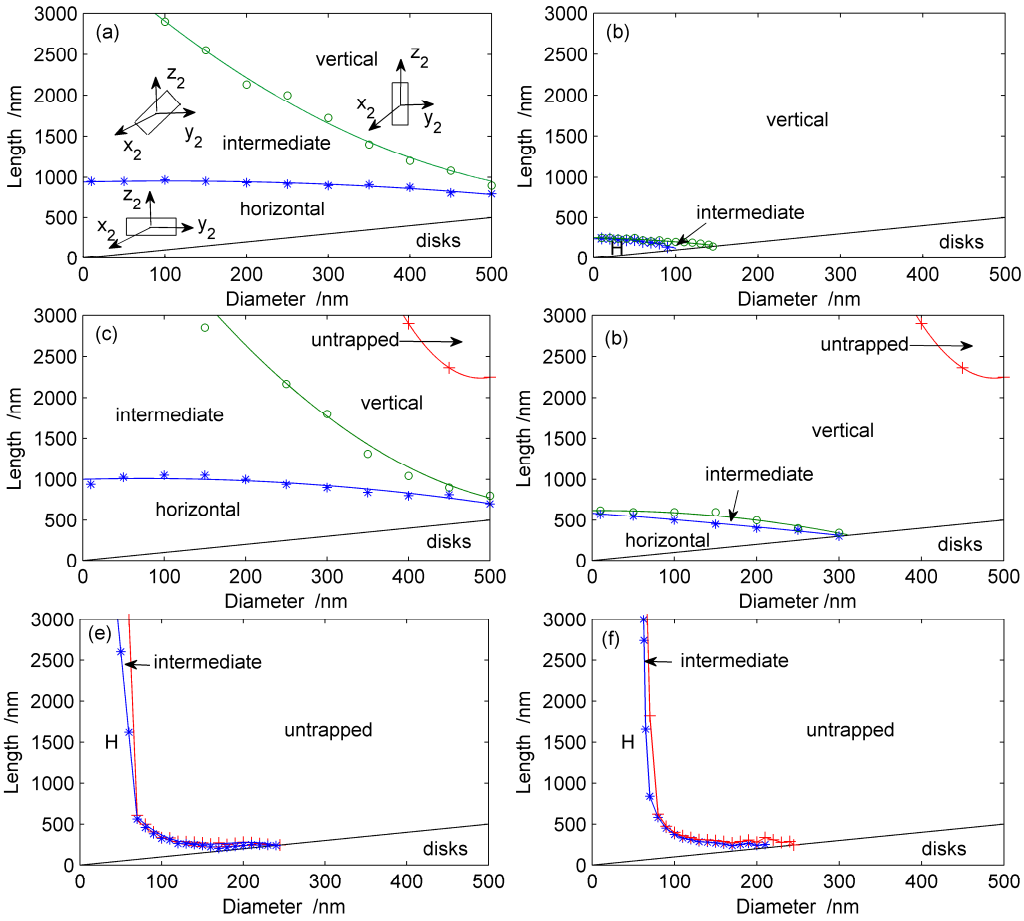

Figure 2. Orientation landscapes of micro- and nano-cylinders with different refractive indices in (a, c, e) linearly and (b, d, f) polarized beams. The refractive indices are (a, b) 1.38, (c, d) 1.57 and (e, f) 3.5498. "H" represents horizontal orientation. The "star" means the longest nanowire or microcylinder trapped horizontally for each diameter. The "circle" represents the shortest nanowire or microcylinder trapped vertically for each diameter. The "cross" indicates the shortest nanowire or microcylinder for each diameter, which cannot be trapped (vertically). The fitting curves are used to distinguish different regions.

There is a big difference in the orientation landscapes of cylinders with a refractive index of 1.38 or 1.57 between linear and circular polarizations. For cylinders with the same refractive index, the horizontal and intermediate regions are smaller for circular polarization when compared to corresponding regions for the linear polarization. The vertical orientation region becomes larger for circular polarization. This means that the rods trapped with stable horizontal orientation or with a tilt angle in a linear polarized beam may be trapped vertically in the beam with circular polarization. The linear polarization contributed to the horizontal torque component which would make the rod lie down. However, the circular polarization made the time-averaged horizontal torque component so weak that the rod stands up. The difference of orientation regions between linear and circular polarizations for silicon cylinders is very small. There is no vertical region for these cylinders. The orientations of the cylinders with sizes around the intermediate region are very sensitive. Polarizations clearly have a strong effect on the orientation of cylinders. However, polarizations do not dictate whether a particle can be trapped or not.

3.2 multiple-particle systems

The model based on the algorithm for multiple scattering (section 2.2) was used to simulate movements of particles. The T-matrices for the particles in multiple-particle systems were calculated using point matching. It was found that if the precision of T-matrices for multiple-particle system was too low, the calculation would fail after several steps. The scattering matrices amplified $|2\mathbf{T}+\mathbf{I}|^2$ were used to check the precision of the T-matrix, where **I** is identify matrix of T-matrix. The sums of each column of $|2\mathbf{T}+\mathbf{I}|^2$ were between 0.99 and 1.01 in our high precision calculations. This shows that our method is numerically stable for non-absorbing particles.

Two-sphere systems were modelled first. Fig. 3 shows the movements of a two-sphere system which was trapped in linear and circularly polarized beams. The spheres were made of glass with a refractive index of 1.57 and with a diameter of 0.5λ. The spheres were initially located at (0.5, -0.5, 2)λ and (-0.5, 0.5, 2)λ. The initial system configuration shifted when the computation was performed. During the calculation, collision detection routines were used to adjust the spheres' positions so that they didn't intersect. The spheres located on the side of the beam axis came toward to the beam axis, and they were then pulled along the beam axis to their final positions where they stuck together. The equilibrium positions in linearly and circularly polarized beams were the same for the two particles, which were (0, 0, -0.06)λ and (0, 0, -1.06)λ respectively. For some particles, the equilibrium position can be before the focal plane [24]. The centre of the particle is before the focal plane, but part of the particle lies after the focal plane as well.

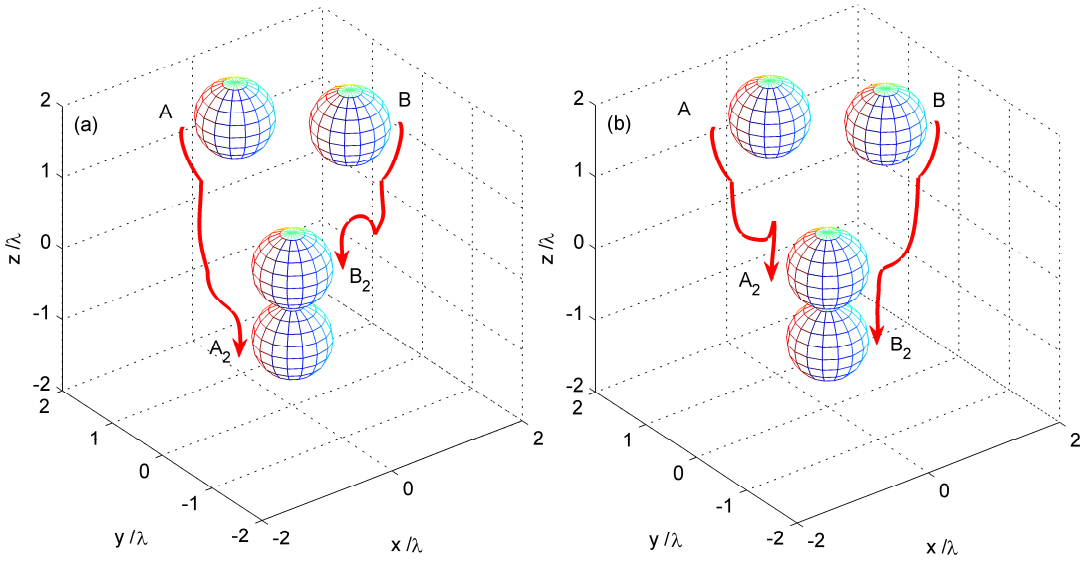

Figure 3. Optical trapping of two spheres in (a) linearly and (b) circularly polarized beams. A and B are the initial positions of the spheres. A_2 and B_2 are the equilibrium positions. Trajectories of the centers of mass of objects are shown by the solid curves and arrows. For the clear view, the curves of trajectories were moved apart.

The algorithm for multiple scattering was also used to calculate the axial forces acting on a single cylinder with a large aspect ratio, which couldn't be calculated using the standard fitting method. We assumed that the cylinder was made up of several short cylinders stuck together. In general, point matching method works well for a single cylinder with an aspect ratio smaller than 2. Fig. 4 shows the force components along *x*-axis and *z*-axis exerted on a cylinder with the radius of 0.25 μm and the length of 1.5 μm when the cylinder was along *z*-axis. The glass cylinder (n = 1.57) was chopped into 2~5 pieces of short cylinders with the same lengths. The beam was linearly polarized along *x*-axis. The force efficiencies calculated using multiple scattering were the sum of the force exerted on each short cylinder. The differences between the *x*-component force curves shown in Fig. 4a are extremely small, which can be considered as the same results. The *z*-component forces in Fig. 4b are not the same. However, the differences between these curves are not large. The calculations converged and could be considered as a having consistent behaviour. Therefore, this model for multiple-particle systems can be considered as a new approximation method. There wasn't any force curve calculated using other methods, because the results obtained using other different methods, such as DDA, FDFD or EBCM were not the same and the differences were not small. This remains an open question about where the different methods apply.

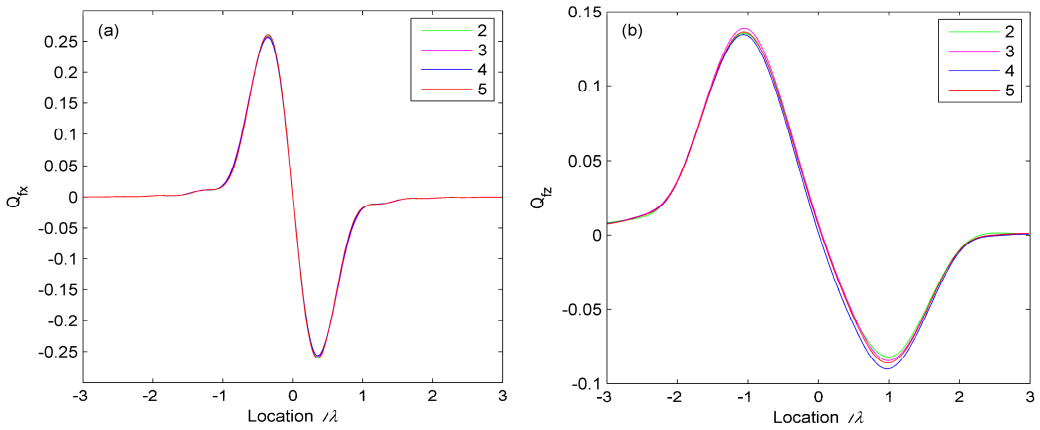

Figure 4. Force efficiency curves of cylinders along (a) *x*-axis and (b) *z*-axis using the model of multiple-particle systems. The radius of the cylinder is 0.25 μm, and the length is 1.5 μm. The cylinder was chopped into different pieces (2~5) of short cylinders.

The method can be used for the cylinders with diameters between 100 nm and λ (800 nm). However, when the method is used to calculate the force on a cylinder with a diameter larger than λ, the results will start to become inaccurate. For instance, Fig. 5 shows the results for the cylinder with a diameter of 1.25 λ and a length of 6.25 λ, which was chopped into 5 pieces. The *x*- and *z*-component force efficiencies exerted on the cylinder were calculated using this model. The *x*-component force curve is not correct. There is a little peak near the focus, which shouldn't exist. The T-matrix of the subcylinder was analysed as shown in Fig. 5b. The sums of each column of $|2\mathbf{T}+\mathbf{I}|^2$ were between 0.96 and 1.01. In general, this level of accuracy is sufficient for single cylinders, but not for multiple-scattering particles. The T-matrix under these conditions is not good enough.

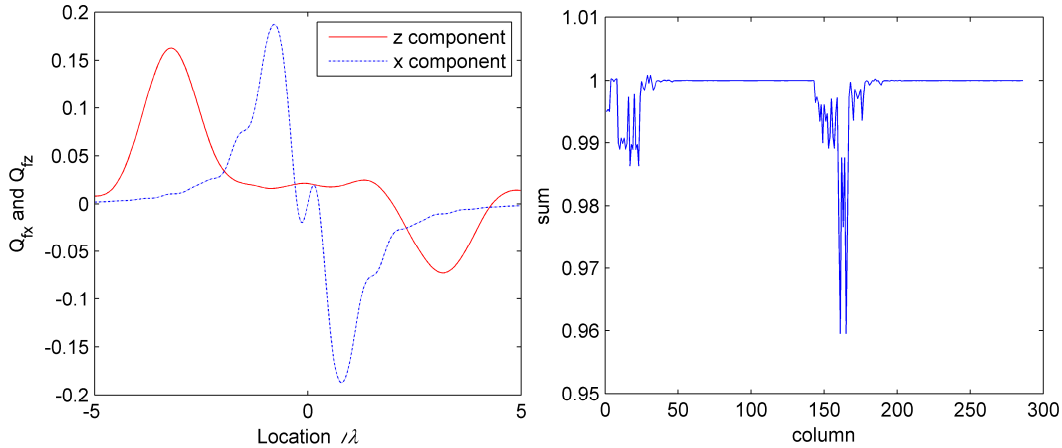

Figure 5. (a) Axial force efficiency curves and (b) the sums of each column of $|2T+I|^2$of the cylinder with a diameter of 1.25 λ and a length of 6.25 λ. The cylinder was chopped into 5 pieces of short cylinders with the same length.

4. CONCLUSIONS

The model for single particles has been presented and used to calculate the orientations of cylinders with different refractive indices. The orientation landscapes of cylinders with diameters between 0 and 500 nm and lengths between 0 and 3000 nm have been presented. There are four regimes in the orientation landscapes of cylinders with aspect ratio larger than one: a horizontal region, vertical region, an untrapped region, and intermediate region between the vertical and horizontal regions. The orientation landscapes of the cylinders with refractive indices of 1.38 and 1.57 demonstrated that the stable orientations of cylinders could strongly depend on the trapping beam polarization. Beam polarizations had little effect on the orientation of cylinders with very high refractive index (3.5498). Apart from these specific results for cylindrical particles, the model is actually a general method for different shaped particles. If the translational and

rotational viscous drag tensors of a shaped particle are known, the method can be used to find equilibrium positions and orientations for the particle in optical tweezers. There are some limitations, such as the lack of drag tensors for some shaped particles. However, it is possible to approximate their drag tensors very simply, such as by using the tensors for a sphere, when the particle is being trapped into its equilibrium position and orientation. The trajectories obtained using this approximation will not be correct, but the equilibrium should be. Even with these limitations, the method presented in this paper provides a useful method for the prediction of equilibriums of many shaped particles.

The model for multiple-particle systems has been developed. The two-sphere system has been simulated when they were trapped into equilibriums. The final stuck configuration has been found in a single tightly focused Gaussian beam. A multi-segment cylinder with aspect ratio of 3 has been calculated using multiple scattering. Results for different numbers of cuts of the same cylinder were quite similar. The model can be considered as a new approximate method to calculate optical trapping of multiple-particle systems. This method works well for multiple-sphere systems. It also has been demonstrated that it can be used for the systems of which the particles are stuck together. The interaction or optical binding in multiple-sphere systems can be investigated using this model. For some kinds of particles the multiple-scattering method doesn't work. The work on multiple scattering is still in the preliminary stages and so not all behaviours, nor all situations where the method is inaccurate have been researched.

ACKNOWLEDGMENTS

This work was supported by the Australian Research Council. The author Yongyin Cao thanks the China Scholarship Council.

REFERENCES

[1] Ashkin A., "Acceleration and trapping of particles by radiation pressure," Phys. Rev. Lett. 24(1), 156-159 (1970).

[2] Harris J., and McConnell G., "Optical trapping and manipulation of live T cells with a low numerical aperture lens," Opt. Express 16(18), 14036-14043 (2008).

[3] Zhong M. C., Zhou J. H., Ren Y. X., Li Y. M., and Wang Z. Q., "Rotation of birefringent particles in optical tweezers with spherical aberration," Appl. Opt. 48(22), 4397-4402 (2009).

[4] Rodriguez-Otazo M., Augier-Calderin A., Galaup J. P., Lamere J. F., and Fery-Forgues S., "High rotation speed of single molecular microcrystals in an optical trap with elliptically polarized light," Appl. Opt. 48(14), 2720-2730 (2009).

[5] Mazolli A., Maia Neto P. A., and Nussenzveig H. M., "Theory of trapping forces in optical tweezers," Proceedings of the Royal Society of London A 459(2040), 3021-3041 (2003).

[6] Neves A. A. R., Fontes A., Pozzo L. de. Y., Thomaz A. A. de, Chillce E., Rodriguez E., Barbosa L. C., and Cesar C. L., "Electromagnetic forces for an arbitrary optical trapping of a spherical dielectric," Opt. Express 14(26), 13101-13106 (2006)

[7] Nakayama Y., Pauzauskie P. J., Radenovic A., Onorato R. M., Saykally R. J., Liphardt J., and Yang P. D., "Tunable nanowire nonlinear optical probe," Nature 447(7148), 1098-1101 (2007).

[8] Neves A. A. R., Camposeo A., Pagliara S., Saija R., Borghese F., Denti P., Iati M. A., Cingolani R., Marago O. M., and Pisignano D., "Rotational dynamics of optically trapped nanofibers," Opt. Express 18(2), 822-830 (2010).

[9] Simpson S.H., Hanna S., "Optical trapping of nanowires," Proc. SPIE 8097, (2011).

[10] Taylor J. M., and Love G. D., "Optical binding mechanisms: a conceptual model for Gaussian beam traps," Opt. Express 17(17), 15381-15389 (2009).

[11] Nieminen T. A., Loke V. L. Y., Stilgoe A. B., Heckenberg N. R., and Rubinsztein-Dunlop H., "T-matrix method for modelling optical tweezers," J. Mod. Opt. 58(5-6), 528-544 (2011).

[12] Loke V. L. Y., Nieminen T. A., Heckenberg N. R., and Rubinsztein-Dunlop H., "T-matrix calculation via discrete dipole approximation, point matching and exploiting symmetry," J. Quant. Spectrosc. Radiat. Transf. 110(14-16), 1460-1471 (2009).

[13] Simpson S. H. and Hanna S., "Application of the discrete dipole approximation to optical trapping calculations of inhomogeneous and anisotropic particles," Opt. Express 19(17), 16526-16541 (2011).

[14] Chaumet P. C. and Billaudeau C., "Coupled dipole method to compute optical torque: Application to a micro-propeller," J. Appl. Phys. 101(2), 023106 (2007).

[15] Nieminen T. A., Heckenberg N. R., and Rubinsztein-Dunlop H., "Calculation of the T-matrix: general considerations and application of the point-matching method," J. Quant. Spectrosc. Radiat. Transf. 79-80, 1019-1029 (2003).
[16] Nieminen T. A., Rubinsztein-Dunlop H., and Heckenberg N. R., "Multiple expansion of strongly focused laser beams," J. Quant. Spectrosc. Radiat. Transf. 79, 1005-1017 (2003).
[17] Cao Y., Stilgoe A.B., L. Chen, Nieminen T. A., and Rubinsztein-Dunlop H., "Equilibrium orientations and positions of non-spherical particles in optical traps," Opt. Express 20(12), 12987-12996 (2012).
[18] Choi C. H., Ivanic J., Gordon M. S., and Ruedenberg K., "Rapid and stable determination of rotation matrices between spherical harmonics by direct recursion," J. Chem. Phys. 111(19), 8825-8831 (1999).
[19] Nieminen T. A., Loke V. L. Y., Stilgoe A. B., Knöner G., Brańczyk A. M., Heckenberg N. R., and Rubinsztein-Dunlop H., "Optical tweezers computational toolbox," J. Opt. A 9(8), S196-S203 (2007).
[20] Purcell E. M., "Life at low Reynolds-number," Am. J. Phys. 45(1), 3-11 (1977).
[21] Bauchau O. A., and Trainelli L., "The vectorial parameterization of rotation," Nonlinear Dynam. 32(1), 71-92 (2003).
[22] Mishchenko M. I., Travis L. D., Mackowski D. W., "T-matrix computations of light scattering by nonspherical particles: A review," J. Quant. Spectrosc. Radiat. Transf. 55, 535-375 (1996).
[23] Delatorre J. G., and Bloomfield V. A., "Hydrodynamic properties of complex, rigid, biological macromolecules - theory and applications," Q. Rev. Biophys. 14(2), 81-139 (1981).
[24] Nieminen T. A., Rubinsztein-Dunlop H., Heckenberg N. R., A.I. Bishop, "Numerical modelling of optical trapping", Comput. Phys. Commun. 142(1-3), 468-471, (2001).